Numerical Simulation of the Integrated Solar/Hybrid Desalination System

Y. Aldali[1], K. Morad[2], Nabil A.S. Elminshawy[2], F. Ahwide[2]

[1]Port Said University, Faculty of Engineering, Egypt
[2]Omar Almokhtar University, Faculty of Engineering,Derna,Libya

e-*mail:* *[1]yasser.aldali@omu.edu.ly;*

Abstract: A mathematical model is developed to predict the performance of the integrated solar/hybrid desalination system. The novel hybrid desalination system in this study consists of multi-stage thermal vapor compression (TVC) system and spiral wound air-gap membrane desalination (AGMD) units. The hot brine rejected from each evaporator stage of TVC system is used as the hot feed to the AGM unit. The parabolic trough collectors (PTCs) field with direct steam generation was considered as solar system. At solar time, the solar field generates a portion of motive steam required to operate the TVC system while the remaining part is generated by the boiler. The results of this study show that the rate of distilled water from TVC system is 3415 L/h (20.56 L/h.m^2) and from the AGMD units is 150 L/h (6.944 L/h.m^2) and the annual saving of natural gas (NG) consumption by using PTCs field is 24 tons. The economic study has indicated that the benefit/cost ratio from of the use of PTCs field to generate a portion of motive steam is 2.1 and the production cost of 1 m^3 of distilled water from AGMD units is 0.9 \$ in comparison with 0.45-2.51 \$ from different types of water desalination systems.

محاكاة عددية لنظام مشترك (هجين) لتحلية مياه البحر بالتكامل مع الطاقة الشمسية

ياسر الدالى [1]   كمال مراد [2] نبيل المنشاوى [2] فرج هويدى [1]

[1]جامعة عمر المختار ـ كلية الهندسة درنة ـ ليبيا

[2]جامعة بورسعيد – كلية الهندسة – جمهورية مصر العربية

ملخص: تم تطوير نموذج رياضي للتنبؤ بأداء نظام تحلية مياه البحر بالتكامل مع الطاقة الشمسية . نظام ألتحلية الهجين المبتكر فى هذه الدراسة يتكون من نظام التبخير الحرارى الانضغاطى متعدد المراحل (TVC) و (AGMD) . المياه المالحة الساخنة المطرودة من كل مرحلة من مبخر نظام (TVC) تستخدم كتغذية ساخنة لوحدة (AGM). المجمعات الشمسية من نوع القطع المكافئ التي

تولد البخار بشكل مباشر استخدمت كنظام شمسي . بوجود الإشعاع الشمسي . الحقل الشمسي يقوم بتوليد جزء من البخار المطلوب لتشغيل نظام (TVC) أما باقي البخار فيتم توليده باستخدام الغلاية . نتائج الدراسة توضح أن معدل المياه المحلاة من نظام ((TVC) (20.56 L/h.m²) 3415 L/h) و من وحدات (6.944 L/h.m²) AGMD) 150L/h)ونتيجة لذلك فان قيمة الوفر السنوي للغاز الطبيعي (NG) المستهلك المتحصل عليها عن طريق استخدام المجمعات الشمسية من نوع القطع المكافئ (PTCs) هي. 24 tons أيضا الدراسة الاقتصادية أشارت الى أن نسبة الفائدة / التكلفة من استخدام مجمعات القطع المكافئ الشمسية لتوليد جزء من البخار بلغت 2.1 وتكلفة إنتاج 1m³ من المياه المحلاة عن طريق وحدات AGMD هي0.9 $ بالمقارنة مع 0.45-2.51 $ من مختلف أنواع أنظمة تحلية مياه البحر.

Keywords: *Integrated solar-hybrid desalination system, parabolic trough collectors, thermal vapor compression, air-gap membrane, benefit/cost ratio.*

1. INTRODUCTION

Global demand for water continues to increase whilst freshwater sources are becoming more scarce due to increasing demand for natural resources and the impacts of climate change, particularly in semi-arid and coastal/island areas. Desalination of seawater and brackish water can be used to augment the increasing demand for fresh water supplies. In some regions – especially the Middle East and Northern Africa (MENA), desalination has become the most important source of water for drinking and agriculture. Desalination demand was projected to expand rapidly. The global demand is projected to grow by 9% per year between 2010 and 2018, with a cumulative investment of about USD 88 billion. In the MENA region, water demand is expected to increase from 9 billion m³ in 2010 up to 13.3 billion m³ in 2030 while groundwater resources are projected to decrease.[1].

Commercial desalination systems can be classified into two main design categories, mainly thermal and membrane types [2]. Thermal designs include multistage flash (MSF), multiple-effect distillation (MED), vapor compression (VC) and low temperature evaporation (LTE). In all these processes, condensing steam is used to supply the latent heat needed to vaporize the water. Vapor compression (VC) may be single or multi-stage distiller in order to improve its efficiency. The vapor is compressed either by a mechanical compressor (mechanical vapor compression, MVC) or by a steam ejector (thermal vapor compression, TVC). For TVC, motive steam at higher pressure is withdrawn from another process, e.g. a steam power cycle or industrial process steam. Owing to their high-energy requirements, thermal processes are normally used for seawater desalination [3].

Membrane designs fall into two types based on the driving force for mass transfer; membrane distillation (MD) which is a thermally driven membrane separation process that involves evaporation of the volatile constituents through a hydrophobic, microporous membrane. The driving force for mass transfer is the vapor pressure difference (induced mainly by temperature difference) across the membrane, rather than hydraulic pressure difference (second type) used in reverse osmosis (RO) [4] and nanofiltration (NF) [5].

Four basic process configurations exist in MD to facilitate evaporative mass transport across the membrane [6]. These include direct contact MD (DCMD), vacuum MD (VMD), air-gap MD (AGMD), and sweep-gas MD (SGMD) [7]. A recent new configuration that synergistically combines elements of DCMD and VMD (termed vacuum enhanced DCMD (VEDCMD)) demonstrated that water flux could be almost doubled compared to DCMD operated at similar temperatures and flow rates [8,9]. Similar to thermal distillation processes, phase change during the MD separation process results in a very pure product water compared to other membrane desalination designs (RO and NF) in which solutes also diffuse through the membrane.

Hybrid systems combining thermal and membrane processes are being studied as promising options. Hybrid plants have potential advantages of a low power demand resulting in a lower operative cost as compared to stand alone thermal or membrane plants. Several models have already been described in the literature to find an efficient relationship

between both desalination processes. Various MSF/RO combinations were reviewed by Al-Mutaz [10]. He discussed the current status, the potential advantages, and the future trends of MSF/RO hybrid desalination systems. In recent years, the concept of MSF/RO configuration has been applied to a number of existing or new commercial desalination plants. The Saline Water Conversion Corporation (SWCC) in Jeddah, Al-Jubail and Yanbu existing Power/Water cogeneration plants were expanded for more water production by combining with new RO desalination plants. The simple hybrid desalination arrangement enabled the increase of water to power ratio and utilized effectively the available intake/outfall facilities. A large hybrid RO/MSF desalination plant was recently built in Fujairah, UAE (April 2004, 284,000 cubic meters per day from MSF and 171,000 cubic meters per day from RO) [11].

Desalination processes require significant quantities of energy to achieve separation of salts from seawater, requiring mainly water vapor for MSF, MED, and VC, hot feed water for MD, and high-pressure pumping power for RO and NF. Traditionally, fossil fuels such as oil and gas have been the major energy sources. The dramatic increase of desalinated water supply will create a series of problems, the most significant of which are those related to energy consumption and environmental pollution caused by the use of fossil fuels. Renewable energy systems produce energy from sources that are freely available in nature. Current information on desalination shows that only 1% of total desalinated water is based on energy from renewable sources [1 , 12]. Among the potential sources of renewable energy, solar/seawater desalination plants are considered to be one of the most economic. Solar/seawater desalination is growing especially in arid regions with huge solar energy potentials such as the MENA region. However, these regions are subject to variable solar intensities while desalination processes are designed for continuous operation

Therefore, the main objective of this study is to present the mathematical model to simulate and analyze the performance of a proposed new hybrid

desalination system located at Port Said city in Egypt 31.26°N latitude and 32.28°E longitude and it is situated at 6 meters above sea level.

The climate data including daily DNI, ambient temperature, wind speed, atmospheric pressure, sun angle and solar azimuth angle for the complete year have been used to evaluate the performance of the integrated solar/hybrid desalination system. Egypt receives a high range of solar DNI range, where the DNI varies from 5.2 kW h/m²/day to 7.6 kW h/m²/day. Port Said has been chosen in this analysis due to its favorable condition for parabolic trough collector technology. An annual average of 2045 kW h/m²/year DNI is received in Port Said city. See Figure 1.
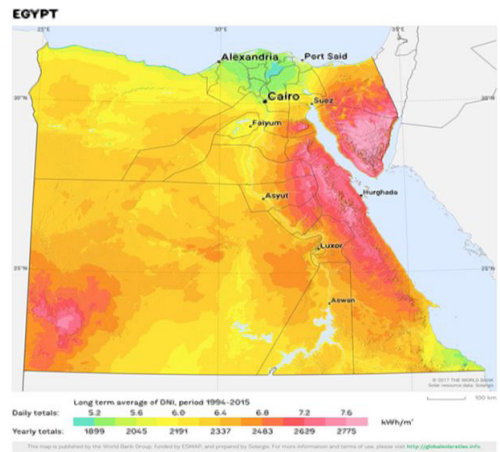

Figure (1). Direct solar irradiance (DNI) for Egypt [15].

The system consists of multi-stage TVC and AGMD processes with solar assist as promising options. The parabolic trough collectors (PTCs) field with direct steam generation is considered as solar system. The economic study includes the benefit of using AGMD units by comparing the cost of 1 m³ of distilled water obtained from AGMD units with price of distilled water from other desalination systems. The economic study also deals with the economic impact of using PTCs field in the form of benefit/PTC field cost ratio to justify the substitution potential of such clean energy.

2. SYSTEM DESCRIPTION

A schematic diagram of the proposed integrated solar TVC/AGMD system is given in Fig. 1. The system constitutes a PTC solar field, TVC unit includes an evaporator of three stages, condenser and steam ejector, and AGMD units. The mass flow rates at different points are also given in Fig. 1. The system operates with constant rate of motive steam. At solar time, the solar field generates a portion of motive steam ($\dot{m}_{m,s}$) while the remaining part ($\dot{m}_{m,b}$) is generated by the boiler. As shown in Figure 1, the brine rejected from each stage of the evaporator is used as the feed while the seawater at inlet temperature of 25°C is used as coolant to the AGMD units.

2.1 Parabolic Trough Solar Collectors

The heat transfer model determining the performance of the parabolic trough solar collectors is based on an energy balance about the absorber tube and glass envelope. The energy balance includes the direct normal solar irradiation incident on the collector, optical losses from both the absorber tube and glass envelope, thermal losses from absorber tube, and the heat gain into the heat transfer fluid (HTF). The concept of DSG is to use water as a HTF so that the solar field preheats and evaporates the water feed to the solar collectors. Detailed description of the numerical model to calculate the performance of the solar collector field can be found in Aldali et al. [13] and Aldali and Morad 14]. The portion of the mass flow rate of the motive steam generated from the solar field is given by

$$\dot{m}_{m,s} = \frac{\dot{Q}_{net}}{C_p(T_s - T_i) + h_{fg}} \quad \text{............................. (1)}$$

where: $\dot{Q}_{net}$ is the net rate of heat gain into the water, C_p is the specific heat of water, T_s is the saturated temperature corresponding to motive steam pressure, T_i is the water inlet temperature which is the saturated temperature corresponding to supply pressure (P_s) to the first stage of the evaporator of the TVC system, and h_{fg} is the latent heat of vaporization corresponding to motive steam pressure. The net rate of thermal energy gained to the water is given by
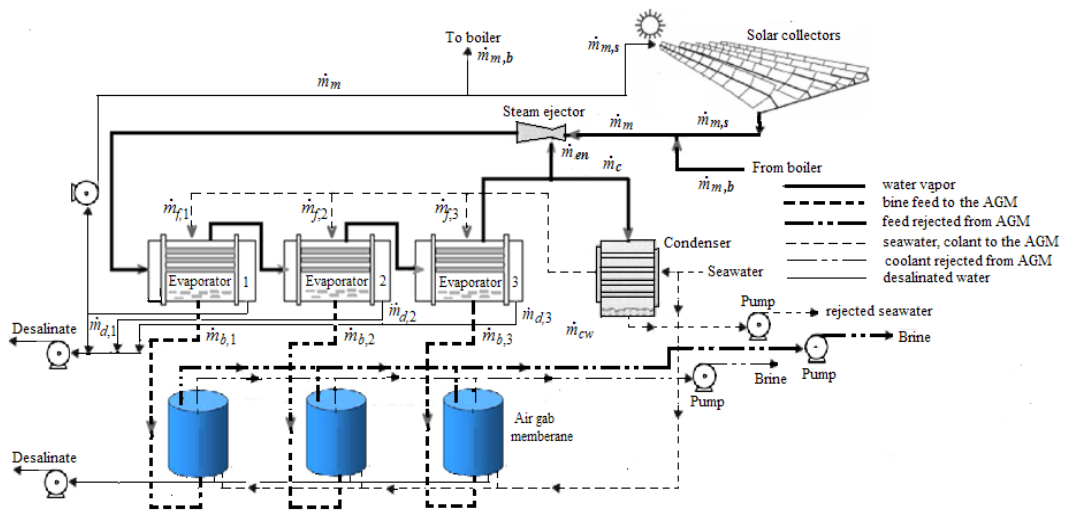
Figure (2). A schematic diagram for the integrated solar TVC/spiral wounded AGM desalination system.

$$\dot{Q}_{net} = \dot{Q}_{in} - \dot{Q}_{loss} \quad \text{... (2)}$$

Where: $\dot{Q}_{in}$ is the effective incoming solar power which is absorbed by selective coating of the absorber tube and $\dot{Q}_{loss}$ is the thermal power loss from the absorber tube which is given by

$$\dot{Q}_{loss} = \pi\, D_o L N h_{comb} \left(T_{ab} - T_{gc} \right) \quad\text{...................} \quad (3)$$

where D_o, L, and N are the outer diameter, total length and number of the absorber tubes, respectively, h_{comb} is the combined heat transfer coefficient (convection and radiation) from the absorber tube to the glass envelope, T_{ab} is the absorber tube temperature, and T_{gc} is the glass cover temperature. Detailed calculations of h_{comb}, T_{ab}, and T_{gc} can be found in Aldali et al. [13]. These calculations were based on the neglecting of conduction resistance of the absorber tube and the heat losses from absorber tube support bracket. The solar power input to the absorber tubes, $\dot{Q}_{in}$, is given by

Table (1). Parameters and operating conditions of the PTCs field [13]

Physical dimensions of collector	
Absorber tube inner diameter	50 mm
Absorber tube outer diameter	70 mm
Glass envelope inner diameter	85 mm
Glass envelope outer diameter	90 mm
Aperture presented by one collector	5.76 m
Solar collector Absorber tube length	5.6 m
Optical properties of collector material	
Transmissivity of glass envelope	0.85
Emissivity of glass envelope	0.88
Emissivity of absorber tube	0.05
Absorptivity of absorber tube	0.95
Environmental/thermodynamic conditions	
Ambient temperature	25°C
Wind speed	0.5 m/s
Pressure of saturated steam	750 kPa
Enthalpy of input water	282 kJ/kg
Maximum mass flow rate of steam	0.075 kg/s

$$\dot{Q}_{in} = A_c \rho_{mirror} I_{solar}\, \tau\alpha \quad\text{...................................} \quad (4)$$

Where: A_c is the total collector area (m^2), ρ_{mirror} is the reflection coefficient of the mirror, I_{solar} is the beam irradiance (W/m^2), τ is the transmissivity of the glass envelope, and α is the absorptivity of the absorber tube. Table 1 lists physical dimensions of each collector, physical properties of the material used in the collector construction and environmental/thermodynamic conditions [15]. For this study, the monthly hourly average global solar radiation on the horizontal plane was made available for Port Said by NASA website. In this study, the solar field consists of one standard loop with 7 collectors in the loop. The length of each collector is 5.6 m and the total length of the loop is 39 m with total area of the PTCs of 224.64 m^2.

2.2 Multi-Stage TVC System

The TVC desalination system consists of evaporator of three stages, the steam jet ejector, and the condenser. Each stage of the evaporator consists of an evaporator/condenser heat exchanger, a vapor space, water distribution system, and a mist eliminator. On the other hand, the steam jet ejector is composed of a steam nozzle, a suction chamber, a mixing nozzle, and a diffuser. The characteristics and the range of the operating conditions for the TVC system are listed in Table 2.

Within the evaporator, the supplied steam flows and condenses inside the tubes and the feed salient water coming from the condenser at T_f is sprayed at the top where it falls in the form of thin film down the succeeding rows of tubes arranged horizontally. In each stage of the evaporator, the latent heat of condensation of the supplying steam is used to evaporate a portion of the feed salient water. In the first stage of the evaporator, the supplied steam is the summation of the motive and the entrainment steams $(\dot{m}_m + \dot{m}_{en})$ coming from the steam ejector, while the steam generated from the first stage is considered as the supplied to the second stage and the steam generated from the second stage is used as the supplied to the third stage.

The distillate and rejected brine flow rates for each stage of the evaporator are obtained by applying mass and salt balance equations. The two balance equations which assume that the distillate water is salt free are given by

Table (2). Parameters and operating conditions of the TVC unit [15]

Compression ratio, CR 2.5	2.5
Boiling temperature, T_b	40 -110°C
Motive steam pressure, P_m	250-1500 kPa
Intake seawater salinity, X_f	42,000 ppm
Intake seawater temperature, T_{cw}	25°C
Brine reject concentration, X_b	70,000 ppm
Feed seawater temperature, T_f	T_b – 5°C
Condenser efficiency, h_c	0.9
Evaporator stage heat transfer area, A_e	37.1 m²
Heat transfer area for the condenser, A_c	54.8 m²

$$\dot{m}_{f,i} = \dot{m}_{d,i} + \dot{m}_{b,i} \quad .... \quad (5)$$

$$\frac{\dot{m}_d}{\dot{m}_f} = \frac{X_b - X_f}{X_b} \quad .... \quad (6)$$

where: $\dot{m}$ is the mass flow rate, X is the salinity, the subscripts i, b, d, and f denote the number of evaporator stage (1, 2, or 3), rejected brine, distillate, and feed seawater, respectively. As shown in Table 1, the salinity of rejected brine, X_b, is considered as constant value, therefore, the ratio $\frac{\dot{m}_d}{\dot{m}_f}$ is the same for the three stages of the evaporators.

The generated vapor from each stage of the evaporator is at the saturation temperature, T_v, which corresponds to the pressure in the stage vapor space. This temperature is less than the boiling temperature T_b by the boiling point elevation BPE due to the salts dissolved in the water, where,

$$T_b = T_v + PBE \quad .... (7)$$

The BPE depends upon the boiling temperature and the salinity of the rejected brine for each stage. A correlation of BPE is given by [15]

$$PBE = AX_b + BX_b^2 + CX_b^3 \quad .... \quad (8)$$

where

$$A = 8.25431 \times 10^{-5} + 1.883 \times 10^{-8} T_b + 4.02 \times 10^{-10} T_b^2$$
$$B = 7.625 \times 10^{-12} + 9.02 \times 10^{-13} T_b - 5.2 \times 10^{-15} T_b^2 \quad .... \quad (9)$$
$$C = 1.522 \times 10^{-15} - 3 \times 10^{-18} T_b - 3.0 \times 10^{-20} T_b^2$$

Neglecting the saturation temperature depression associated with pressure losses in the demister, the temperature of saturated vapor leaving each stage of the evaporator, T_{ev}, is considered equal to the saturated temperature in the stage vapor space, T_v.

In each stage of the evaporator, the supplied dry saturated steam is used to raise the temperature of the feed seawater m_f from the inlet temperature T_f to the boiling temperature T_b. In addition, it supplies the latent heat required to evaporate the specified mass of vapor, m_v. The energy balance equations for the three stages of the evaporators are written as

$$\dot{Q}_{ev,i} = \dot{m}_{f,i} C_p (T_{b,i} - T_f) + \dot{m}_{vi} h_{fg,vi} = \dot{m}_{si} h_{fg,si}$$
$$= U_{ev} A_{ev} (T_s - T_{b,i}) \quad .... \quad (10)$$

Where $\dot{Q}_{ev,i}$ is the thermal load of each stage of the evaporator, C_p is the specific heat at constant pressure of the brine, U_{ev} is the overall heat transfer coefficient for the evaporator stage, A_{ev} is the heat transfer surface area for each evaporator stage, h_{fg} is the latent heat of evaporation, si denotes the supply steam to each evaporator stage and vi denotes the generated vapor from each evaporator stage. The overall heat transfer coefficient in the evaporator stage is calculated as a function of boiling temperature for each stage from the following correlation [15]

$$U_{ev} = \begin{pmatrix} 1969.5 + 12.05T_b - 0.85989 \times 10^{-1} T_b^2 \\ 0.25651 \times 10^{-3} T_b^3 \end{pmatrix} \times 10^{-3} \quad ...(11)$$

The condenser is a counter-current surface condenser in which the seawater $(\dot{m}_{cw} + \dot{m}_f)$ is introduced into the tube side of the condenser. After being heated in the condenser, the seawater stream leaving the condenser is divided into two parts. The first and smaller part, $(\dot{m}_f)$, is divided between evaporator stages and the second and the larger part, $(\dot{m}_{cw})$, is rejected from the system. A fraction of steam generated in the third stage of the evaporator, $(\dot{m}_{en})$, is entrained by the steam ejector while the condenser operates on the remaining part, $(\dot{m}_c)$. The energy balance equation for the condenser is written as

$$\dot{Q}_c = \dot{m} h_{fg,v3} = (\dot{m}_f + \dot{m}_{cw}) C_p (T_f - T_{cw}) = U_c A_c \Delta T_{ln} \quad .. (12)$$

Where $\dot{Q}_c$ is the thermal load, U_c is the overall heat transfer coefficient, A_c is the heat transfer surface area for the condenser, and ΔT_{ln} is the logarithmic

mean temperature difference defined as

$$\Delta T_{ln} = \frac{T_f - T_{cw}}{\ln\left(T_f / T_{cw}\right)} \quad .... \quad (13)$$

The overall heat transfer coefficient in the condenser is calculated as a function of condensing temperature, T_c, which is equal to the temperature of the saturated vapor leaving the third stage of the evaporator, $T_{ev,3}$, by the following correlation [15]

$$U_c = \begin{pmatrix} 1719.4 + 3.2063 T_c + 1.597 \times 10^{-2} T_c^2 \\ - 1.9918 \times 10^{-4} T_c^3 \end{pmatrix} \times 10^{-3} \quad ..(14)$$

The main data required from analyzing the steam jet ejector is the determination of the mass of motive steam required per unit mass of the entrained vapor (R_a), given the pressure of the motive steam (P_m), compression ratio (P_s/P_{en}) and the suction pressure (P_{en}). Al-Juwayhel [15] developed the following relationships to evaluate the entrained ratio of the steam jet ejector

$$R_a = \frac{\dot{m}_m}{\dot{m}_{en}} = 0.296 \frac{P_s^{1.19}}{P_{en}^{1.04}} \left(\frac{P_m}{P_{en}}\right)^{0.015} \left(\frac{PCF}{TCF}\right) \quad .... \quad (15)$$

Where P_s is the discharge pressure, PCF is the motive steam pressure correction factor and TCF is the entrained vapor temperature correction factor. The following two equations were given to calculate both PCF and TCF [15].

$$\begin{pmatrix} PCF = 3 \times 10^{-7} P_m^2 - 9 \times 10^{-4} P_m + 1.6101 \\ TCF = 2 \times 10^{-8} T_{en}^2 - 6 \times 10^{-4} T_{en} + 1.0047 \end{pmatrix} \quad ...... \quad (16)$$

Where P_m is in kPa and T_{en} is in °C. A detailed analysis of the steam jet ejector can be found in Al-Juwayhel [15].

Performance of the TVC is determined in terms of the amount of fresh water product per unit mass of motive steam, which is called the performance ratio, PR.

$$PR = \frac{\dot{m}_d}{\dot{m}_m} \quad .... \quad (17)$$

where $\dot{m}_d$ is the summation of the distilled water from the three stages of the evaporator,

$$\dot{m}_d = \sum_{i=1}^{3} \dot{m}_{vi} \quad .... \quad (18)$$

The mathematical expressions established during the characterization of individual components of the TVC system are programmed in a subroutine using a Fortran language.

2.3 Spiral Wound AGMD Modules

A novel aspect of this study is the use of the spiral-wound AGMD module, which is more energy efficient compared to most other MD configurations. A schematic diagram of a typical spiral wound AGMD module is illustrated in Figure 4. The system consists of a micro porous hydrophobic membrane sheet situated between hot feed solution and the air gap. In between the air gap width and the cooling channel is a condensation surface. The membrane module contained 7.2 m² of low-density polyethylene membrane having nominal pore size of 0.3 μm [16]. Key characteristics of the commercial spiral wound AGMD module used in this study are provided in Table 3.

Table (3). Characteristics of the spiral wound AGMD module [18].

Total net membrane surface area	As	7.2 m²
Diameter of the module	d	0.4 m
Height of the module	h	0.5 m
Length of envelope	L	1.5 m
Width of envelope	w	0.4 m
Thickness of flow channels	dch	2.0 mm
Porosity of the membrane material	em	0.85
Membrane turtosity	tm	1.56
Porosity of spacer	esp	0.78
Membrane thickness	dm	76.0 μm
Thickness of flow channel	t	2 mm
Air gap width	b	1 mm
Number of evaporator channels	n	6
Number of condenser channels	n	6

The red channels in Figure 3 are the hot feed channels containing a spacer. Both sides of the hot feed channel consist of the membrane. The blue channel is the cold feed channel containing a spacer. Both sides of the cold feed channel consist of the condenser foil. Between each cold and hot feed there is the air gap with spacer in which permeate

is collected and expelled from the module. Water evaporates at the membrane hot feed side and water vapor is transferred through the membrane into the air gap. Inside the air gap the water vapor then condenses onto the condenser foil as permeate. The hot and cold feed are countercurrent. The 6 membrane envelopes are spiral wound into a cylindrical shape, each flat sheet membrane envelope travels tangentially from the inside of the cylindrically shaped module towards the outside

of the cylindrically shaped module. Hence the flow direction in the module is tangentially. To achieve countercurrent in this configuration the hot feed is supplied at the inside (or core) of the module and leaves the module on the outside. The cold feed is supplied at the outside of the module and leaves the module at the core. Hence the core of the module is high in temperature and the outside is cold in temperature effectively making the module self-insulating.
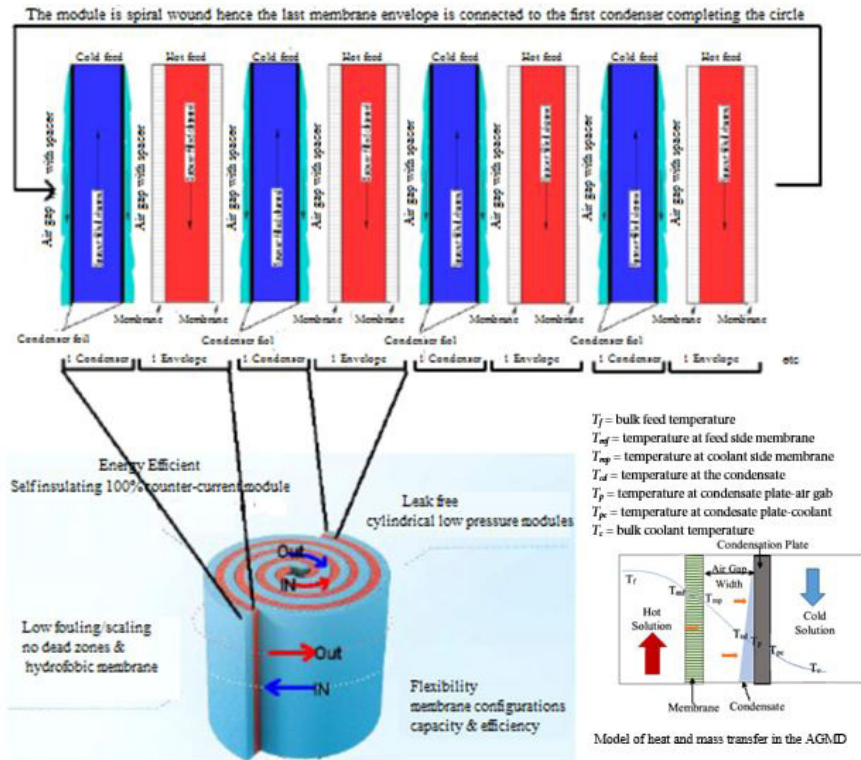

Figure (3). Schematic diagram of a typical spiral wound AGMD module

In modeling the AGMD, the following assumptions are considered: steady state system, air within the membrane pore is considered to be stagnant, constant pressure is considered in the air gap, mass is transferred by diffusion while heat is transferred by conduction within the air gap, no heat exchange between the system and the surroundings, and condensation is film-wise on the cooling plate

The mass transfer across the membrane material depends on the difference in vapor pressure between

both sides of the membrane. The relationship between mass flux and the vapor pressure difference across the membrane is expressed as [16].

$$J_w = \frac{\varepsilon_m PD_{wa}M_v}{RT_m b' P_{a,ln}}(P_{mf} - P_{cd}) \qquad kg/s.m^2 \ldots\ldots (19)$$

Where P_{mf} is the vapor pressure at the feed side of the membrane while P_{cd} is the vapor pressure at the condensate surface $[P_{cd} = Psat(Tcd)]$, R is the universal gas constant (R= 8.314472 kJ/kmol K),

M_v is the molecular weight of the water vapor, T_m is the mean temperature in Kelvin [$T_m = (T_{mf} + T_{cd})/2$], b' is the effective air gap thickness ($b' = d_m \times t_m + b$), D_{wa} is the mass diffusivity between the air and water vapor given by [16]

$$D_{wa} = D_o \left[\frac{T_m}{298}\right]^{2.334} \quad .... \quad (20)$$

Where D_o is the mass diffusivity between the air and the water vapor at standard condition (1 atm and 298 K). For feed solution containing dissolved salt, P_{mf} in Eq. (19) may be estimated using Raoult's law which is given by [16]

$$P_{mf} = (1 - CM_{NaCl})P_{sat}(T_{mf}) \quad .... \quad (21)$$

Where $P_{sat}(T_{mf})$ is the saturated pressure of water vapor at T_{mf} and CM_{NaCl} is the mole solute concentration and can be estimated from

$$CM_{NaCl} = \frac{NaCl_{concentration}(g/L)}{58.44(g/mol)} \quad .... \quad (22)$$

Where 58.44 (g/mol) is the molar mass of sodium chloride. The $P_{a,ln}$ in Eq.(19) is the air pressure in the membrane and it's given by

$$P_{a,ln} = \frac{P_{amf} - P_{acd}}{\ln \dfrac{P_{amf}}{P_{acd}}} \quad .... \quad (23)$$

The transmembrane air pressures P_{amf} and P_{acd} are calculated from the total pressure, P (atmospheric pressure), which is equivalent to the summation of water vapor pressure and air pressure in the membrane bore, therefore,

$$P_{amf} = P - P_{mf} \text{ and } \quad P_{acd} = P - P_{cd} \quad .... \quad (24)$$

In order to obtain the temperatures T_{mf} and T_{cd}, the following heat transfer analysis is considered.

- The transfer of heat from the hot saline solution to the membrane feed surface at steady state can be expressed as [16]

$$\dot{q} = h_f(T_f - T_{mf}) + J_w C_f(T_f - T_{mf}) = h_h(T_f - T_{mf}) \quad ... (25)$$

Where $h_h = h_f + J_w C_f$ and h_f and C_f are the heat transfer coefficient and specific heat of the liquid feed, respectively.

- The heat transfer from the hot membrane surface to the condensate liquid interface takes place due to sensible heat flux, $\dot{q}^s$, and the heat of vaporization at feed membrane surface. It can be expressed as [16]:

$$\dot{q} = h^*(T_{mf} - T_{cd}) + J_w \Delta h_w \quad W/m^2 \quad .... \quad (26)$$

Where Δh_w is the heat of vaporization of water (J/kg) at T_{mf} and h^* is the heat transfer coefficient which is expressed as [16]

$$h^* = \left(\frac{J_w C_{cd}}{1 - e^{\frac{J_w C_{cd}}{h_y}}}\right) \quad W/m^2 K \quad .... \quad (27)$$

Where C_{cd} is the gas phase specific heat capacity and h_y is the gas phase heat transfer coefficient given by $h_y = k/b$ where k is the thermal conductivity of the vapor phase and b is the air gap thickness.

- From the condensate layer interface to the cooling solution, the heat transfer at steady state can be written as [16],

$$\dot{q} = h_d(T_{cd} - T_p) + J_w C_{P,w}(T_{cd} - T_p)$$
$$= \frac{k_c}{l}(T_{cd} - T_{pc}) = h_c(T_{pc} - T_c) = \bar{h}(T_{cd} - T_c) \quad ..... (28)$$

Where h_d is the heat transfer coefficient of the condensate, k_c is the condensate plate thermal conductivity, l is the plate thickness, h_c is the heat transfer coefficient of coolant film and $\bar{h}$ is the overall heat transfer coefficient from vapor/condensate liquid interface to cooling solution and it is expressed as

$$\bar{h} = \left(\frac{1}{h_d^*} + \frac{l}{k_c} + \frac{1}{h_c}\right) \quad W/m^2 K \quad .... (29)$$

where

$$h_d^* = h_d + J_w C_{p,w} \quad W/m^2 \quad .... \quad (30)$$

By considering film-wise condensation, h_d can be estimated from [16]

$$h_d = \left(\frac{g\rho^2 \Delta h_w k_d^3}{L\mu_d(T_{cd} - T_p)}\right)^{1/4} \quad W/m^2 K \quad .... (31)$$

where ρ, k_d, and μ_d are the liquid water density, thermal conductivity, and dynamic viscosity at the condensate film temperature. L is the height of air gap (height of the cooling plate) and g is the acceleration of gravity.

Combination and manipulation of Eq. (19) to (31) leads to

$$\dot{q} = U(T_f - T_c) + \frac{J_w \Delta h_w}{h^*} \qquad W/m^2 \ \text{.................... (32)}$$

$$T_{mf} = T_f - \frac{U}{h_h}\left(T_f - T_c + \frac{J_w \Delta h_w}{h^*}\right) \ \text{......................... (33)}$$

and

$$T_{cd} = T_c + \frac{U}{h_p}\left(T_f - T_c + \frac{J_w \Delta h_w}{h^*}\right) \ \text{....................... (34)}$$

where U is the overall heat transfer coefficient given by

$$U = \left(\frac{1}{h_h} + \frac{1}{h^*} + \frac{1}{h_p}\right)^{-1} \ \text{... (35)}$$

The heat transfer coefficients for the hot and cold fluid sides, h_f and h_c, are estimated using correlations reported by Schock and Miquel [17] for the spiral-wound membrane module

$$Nu = \frac{hd_h}{k} = 0.065 \, Re^{0.875} Pr^{0.25} \ \text{........................ (36)}$$

where $Re = \rho u_m d_h / \mu$ is the Reynolds number and $Pr = \mu C_p / k$ is the Prandtl number. u_m is the mean velocity which is calculated from volume flow rate and d_h is the hydraulic diameter of the flow channel.

The desalinate production rate from spiral-wound AGMD module is given by

$$\dot{V}_d = \frac{J_w A_s \times 3600}{\rho_w} \qquad L/h \ \text{................................ (37)}$$

The performance of a spiral-wound AGMD module can be calculated by solving the set of the above algebraic equations, simultaneously by iteration method. For this a subroutine based on Fortran language is constructed which needs reliable input data regarding geometrical parameters and transport characteristics, initial guess values of the unknown variables, thermophysical and thermodynamic property functions of water and saline solution.

3. VALIDATION OF THE THEORETICAL MODELS

The validation of the TVC mathematical model is checked by comparing the model results for a single-stage evaporator TVC system with data of Al-

Juwayhel [15]. As shown in Figure 4, the performance ratio obtained from the present model is found to be identical to that of the Al-Juwayhel [15].
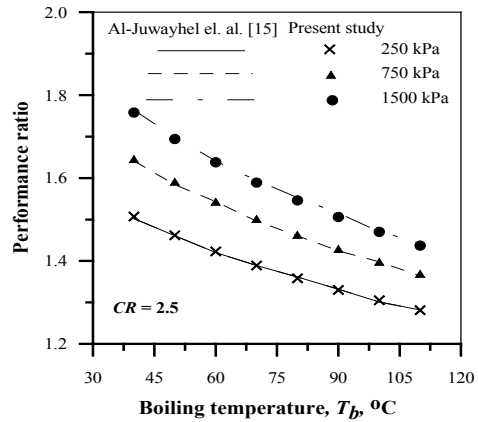

Figure (4). Effect of boiling temperature and the motive steam pressure on the performance ratio of TVC system

The validation of the spiral-wound AGMD mathematical model is checked by comparing the model results with the experimental data of Duong et al. [18] on the variation of distillate production rate with flow rate and temperature for hot feed fluid. The spiral-wound AGMD model simulation results are found to be close to the experimental data as shown in Figure 5.
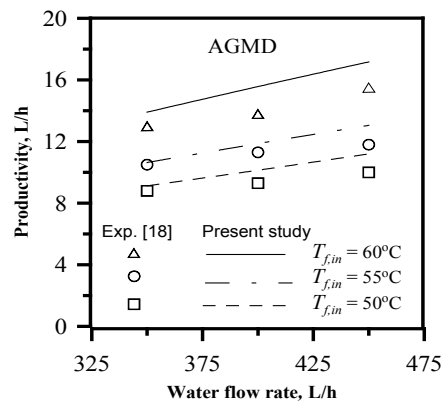

Figure (5). Desalinate product rate of spiral wound AGDM at different feed flow rates and feed inlet temperatures.

4. RESULTS

Figure 6 indicates the effect of the number of evaporator stages on the performance of the TVC system. In this figure, the mass flow rates for both motive and distilled water are plotted against the number of the evaporator stages. The figure shows that the mass flow rate of the motive steam sharply decreases while the mass flow rate of distilled water slightly decreases with the increase of the number of evaporator stages, therefore the performance ratio of the PVC system significantly increases with the increase of the number of evaporator stages. Increasing number of evaporator stages from 1 to 3 decreases the amount of distilled water by 10.2 % while the amount of motive steam decreases by 89.9%. Therefore, the energy required for the TVC system also decreases by 89.9% with using 3-stage evaporator system. The number of evaporator stages is limited to 3 by the temperature difference requirement in the condenser.
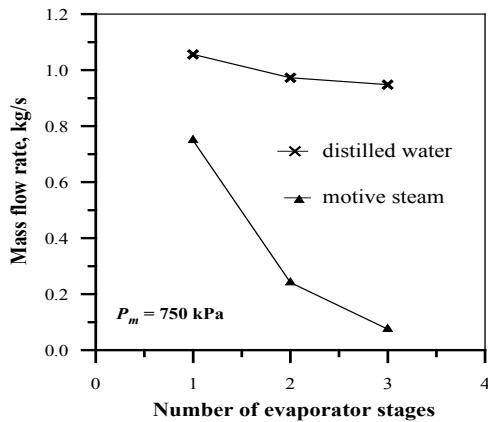

Figure (6). Effect of number of evaporator stages on the mass flow of motive steam and desalinated water of TVC system.

Figure 7 shows the rate of distilled water for both TVC system and AGMD units. The evaporator stage No. 3 gives maximum amount of distilled water (1665 L/h) while the AGMD unit which operates with the brine rejected from the evaporator stage

No.2 gives the maximum amount of distilled water (65 L/h). The total amount of distilled water from TVC system is 3415 L/h (20.56 L/h.m^2) and from the AGMD units is 150 L/h (6.944 L/h.m^2).
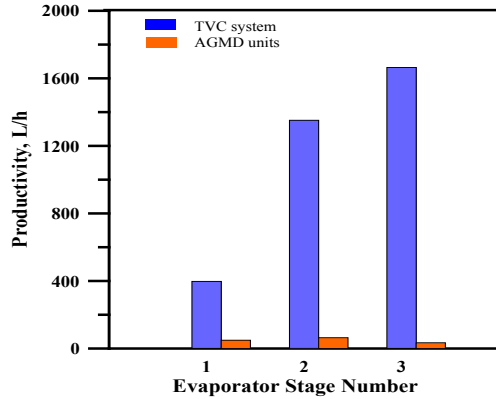

Figure (7). Productivity of distilled water from hybrid desalination system

In the present study, the solar field is considered in operation for 10 h per day (07:30 - 17:30) of usable sunlight during the whole year, Figure 8 shows the hourly average solar motive steam fraction ($\dot{m}_{m,s}/\dot{m}_m$) during solar daytime for three selected months (July, March, and December). As shown in this figure, the fraction reaches unity in July during the 5th and 6th solar hours (11:30 – 13:30). This means that the total amount of motive steam is obtained from the solar field. The maximum and minimum fractions of solar motive steam during solar daytime in March are 0.496 and 0.307 and in December are 0.052 and 0.01, respectively.

If the fuel used in the boiler is a natural gas (NG) of heating value of 57,490 kJ/kg [14] and boiler efficiency of 95% is assumed, the monthly reductions of the NG consumption due to the use of PTCs field are calculated and shown in Figure 10. The minimum saving of NG consumption that is 0.13 ton is in December and the maximum saving of NG consumption is in July that is 3.52 tons. The annual saving of NG consumption by using PTCs field ($\dot{m}_{NG,saving}$) is 24 tons.
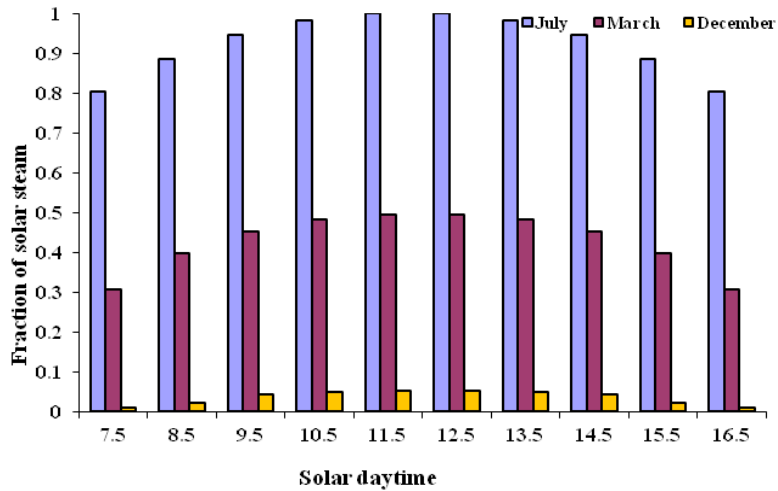
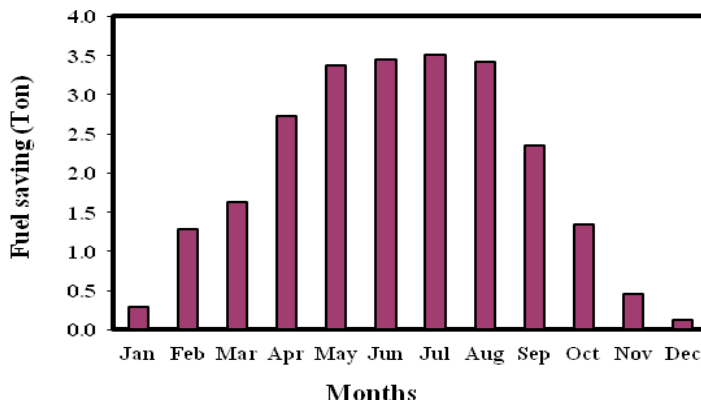**Figure (8). Fraction of solar motive steam during daytime**

Figure (9). Monthly reduction of NG by using PTCs field

5. ECONOMIC STUDY

The preset economic study includes two objectives, the first one is the study of the economy of using PTCs field to generate a portion of motive steam which is relevant to compare the resulted reduction cost of the NG savings to the cost of the solar field which is called benefit/cost ratio. Since the brine rejected from each stage of the evaporator of the PTV system is at higher temperature than that for seawater, therefore, no additional thermal energy is needed for the AGMD units. Then the second

objective of the present economic study is relevant to estimate the cost of distilled water from the AGMD units and compare this cost with that for the other desalination systems.

The PTCs associated with higher initial investment costs and lower operating costs. Relating to collectors area considered in Aldali and Morad [14], the investment cost of solar collectors should be 42,680 $ considering the investment cost of 190 $/m² of the PTCs. The installation cost should be 21,460 $, the control cost should be 10,730 $, and

the supporting material cost should be 24,700 $. Then, the total initial investment cost to install the solar field is approximately 99,570 $. Considering the economic life time of the solar field of 25 years and an annuity interest rate of 10%, then the yearly payment of the initial investment cost is approximately 4,380 $/year [19]. The insurance is supposed to be 2% of the initial investment cost and the O&M costs are assumed to be 4% of the initial investment cost [20], then the resulting annual investment cost is 10,354 $/year. The average national price of the liquefied NG (LNG), CLNG, is 900 $/ton [14], then the annual revenue, RLNG saving, from the LNG saving by using PTCs field is

$$R_{LNG\ saving} = C_{LNG} \times \dot{m}_{NG,\ saving} \qquad \$/year$$

which is approximately 21,600 $/year. From this economic analysis, it is found that the benefit/cost ratio of the PTCs field is approximately 2.1. Furthermore, the use of solar energy will reduce the greenhouse CO_2 emission.

The commercial price of each AGM unit (R_{AGM}) having the specifications listed in Table 3 is approximately 2600 $ and the life span of the AGM unit is 20 years [21]. The capital investment of the water pumps is calculated from the following equation [22];

$$R_{pump} = 13.92\dot{m}_d^{0.55}\Delta P^{0.55}\left(\frac{\eta}{1-\eta}\right)^{1.05} \qquad \$ \quad ....\ (38)$$

where $\dot{m}_d$ is in kg/s, ΔP in kPa, and h is the polytropic pump efficiency (0.75). If the yearly O&M costs including the pumping power cost are assumed to be 10% of the price of AGM units, then the cost of the distilled water from AGMD units is

$$C_{AGMD} = (N \times R_{AGM} + R_{pump})/life\ span + 0.1 \times N \times R_{AGM} \quad \$/Year \ ..(39)$$

where N is the number of AGM units (3). Then the cost of 1 m³ of distilled water from AGMD units is

$$R_{AGMD} = C_{AGMD}/(P_{AGMD} \times 1000) \quad \$/m^3 \ ....\ (40)$$

where P_{AGMD} is the productivity from AGMD units (L/year). From the above analysis, the cost of 1 m³ of distilled water from AGMD units is 0.9 $. The production cost of distilled water from different types of water desalination systems is in the range of 0.45-2.51 $/m³ [23]. The lower cost of distilled water

from AGMD units in the present study is due to the use of hot brine rejected from the evaporator stages of the TVC system as the feed to the AGMD units, therefore no additional thermal energy is required for the hybrid system.

6. CONCLUSIONS

A mathematical model to simulate and analyze the performance of a proposed new hybrid desalination system consisting of multi-stage TVC and AGMD processes with solar assist as promising option is presented in this article. The parabolic trough collectors (PTCs) field with direct steam generation is considered as solar system. The economic study includes the benefit of using AGMD units by comparing the cost of 1 m³ of distilled water obtained from AGMD units with price of distilled water from other desalination systems. The economic study also includes the study of economic impact of using PTCs field in the form of benefit/PTC field cost ratio to justify the substitution potential of such clean energy. The main conclusions of this task are:

- The increase of evaporator stages of the PTV system from 1 to 3 decreases the amount of distilled water by 10.2% while the amount of motive steam decreases by 89.9%.

- The productivity of the distilled water from TVC system is 3415 L/h (20.56 L/h.m²) and from the AGMD units is 150 L/h (6.944 L/h.m²).

- The annual saving of NG consumption by using PTCs field is 24 tons.

- The benefit/ cost ratio by using PTCs field to generate a portion of motive steam is 2.1.

- The production cost of 1 m³ of distilled water from AGMD units is 0.9 $ in comparison with 0.45-2.51 $ from different types of water desalination systems.

6. NOMENCLATURES

A	area, m²
CP	specific heat at constant pressure, J/kg. K
D	diameter (m), diffusion coefficient, m²/s

h	heat transfer coefficient $W/m^2. K$
$\overline{h}$	overall heat transfer coefficient, $W/m^2. K$
hfg	heat of vaporization, kJ/kg
Hu	lower heating value, kJ/kmol
I_{solar}	beam irradiation, W/m^2
J	mass flux, $kg/s.m^2$
k	thermal conductivity, W/m.K
L	total length of the absorber, m
$\dot{m}$	mass flow rate, kg/s
M	molecular weight, kg/kmol
N	number of absorber tubes
P	pressure, N/m^2
PR	performance ratio
$\dot{Q}$	rate of heat transfer, kW
U	overall heat transfer coefficient, $W/m^2.K$
T	temperature, ^oC
ΔT_{ln}	log-mean temperature difference, ^oC
X	salinity
Greeks	
α	absorpitivity of the absorber tube
μ	dynamic viscosity, kg/m.s
ρ	reflectivity of the mirrors, density
τ	transmissivity of the glass cover
Subscripts	
ab	absorber
b	brine
c	collector, condenser, condensate plate, coolant
cd	condensate surface
comb	combined
cw	cooling water
d	distilled
en	entrained vapor
ev	evaporator
gc	glass cover
f	feed
i	inlet, stage number
in	incoming solar power
m	mean , motive steam

m,b	boiler motive steam
mf	membrane feed side
mp	air-gap side membrane
m,s	solar motive steam
o	outer
p	plate
pc	condensate plate-coolant side
s	supply, saturation condition
v	vapor
w	water
Abbreviations	
AGMD	air-gap membrane distillation
DCMD	direct contact membrane distillation
HTF	heat transfer fluid
MD	membrane distillation
MED	multi-effect distillation
MSF	multistage flash
MVC	mechanical vapor compression
PTCs	parabolic trough collectors
RO	reverse osmosis
TVC	thermal vapor compression

7. REFERENCES

[1]. IEA-ETSAP and IRENA, 2012, "Water Desalination Using Renewable Energy," Technology Brief I12 – March 2012, www.etsap.org – www.irena.org

[2]. International Atomic Energy Agency, 2006, "Desalination Economic Evaluation Program, (DEEP-3.0)," IAEA, VIENNA, 2006, IAEA-CMS-19.

[3]. El-Ghonemy, A.M.K., 2012,"Future sustainable water desalination technologies for the Saudi Arabia: A review," Renewable and Sustainable Energy Reviews, Vol. 16, pp. 6566-6597.

[4]. Cath, T.Y., 2010, Osmotically and thermally driven membrane processes for enhancement of water recovery in desalination processes," Desalination and Water Treatment, Vol. 15, 279-286.

[5]. Zhou, D, Zhu, L, Fu, Y, Zhu, M, and Xue, L, 2015, "Development of Lower Cost Seawater Desalination Processes Using Nano-Filtration Technologies — A review," Desalination, Vol. 376 pp. 109–116.

[6]. Wilf, M.,2006, "The Guidebook to Membrane Desalination Technology," by L.Awerbuch, published M. Balaban, Desaliantion Publication Science and Technology. Park of Abruzzo, 2006

[7]. Khawaji, A.D., Kutubkhanah, I.K., and Wie, J.M., 2008, "Advances in Seawater Desalination Technologies," Desalination, Vol. 221, pp. 47–69.

[8]. Cath, T.Y., Adams, V.D., and Childress, A.E., 2004, "Experimental Study of Desalination Using Direct Contact Membrane Distillation: a New Approach to Flux Enhancement," J. Membr. Sci., Vol. 228, pp. 5–16.

[9]. Martinetti, C.R., Childress, A.E., and Cath, T.Y., 2009, "High Recovery of Concentrated RO Brines Using Forward Osmosis and Membrane Distillation," J. Membr. Sci., 331 (2009) 31–39.

[10]. Al-Mutaz, I.S., 2005, "Hybrid RO MSF Desalination: Present Status and Future Perspectives," 2nd Forum on: Water Desalination and Purification Technology Outlook for the Arab World & Non-Governmental Organizations Forum, University of Sharjah, UAE, 8 - 10 May.

[11]. Osman A. Hamed, 2004, "Overview of Hybrid Desalination Systems - Current Status and Future Prospects," International Conf. on Water Resources & Arid Environment (2004)

[12]. Li, C., Goswami, Y., and Stefanaks, E. 2013, "Solar Assisted Sea Water Desalination: A Review," Renewable and Sustainable Energy Reviews, Vol. 19, pp. 136-163.

[13]. Aldali, Y., Davison, B., Muneer, T., Henderson, D., 2012, " Modeling the behavior of a 50 MW direct steam generation plant for southern Libya based on the thermodynamic and thermophysical properties of water substance," transaction of the ASME, J. Sol. Energy Eng. 134 (4) (2012) 041001-1– 041001-9, http://dx.doi.org/10.1115/1.4006893.

[14]. Aldali, Y., Morad, K., 2016, "Numerical simulation of the integrated solar/North Benghazi combined power plant," Applied Thermal Engineering 108 (2016) 785– 792.

[15]. Al-Juwayhel, F., El-Dessouky, H., Ettouney, H., 1997, "Analysis of Single-Effect Evaporator Desalination Systems Combined with Vapor Compression Heat Pumps," Desalination, Vol. 114, pp. 253-275.

[16]. Lawal, D.U., 2014, "Desalination Using Air Gap Membrane Distillation," Master of Science, King Fahd University of Petroleum & Minerals, Dhahran, Saudi Arabia.

[17]. Schock G., Miquel, A., 1987, "A Mass transfer ad Pressure loss in Spiral Wound Modules," Desalination 64, pp. 339-352.

[18]. Duong, H.C., Chivas, A.R., Nelemans, B., Duke, M., and Gray, S., 2015, "Treatment of RO brine from CSG produced water by spiral-wound air gap membrane distillation — A pilot study," Desalination 366, pp. 121–129.

[19]. Aldali, Y., Morad, K., 2014, "Thermal Performance improvement of Derna Electric Power Station (Unit 5) Using Solar Energy," Journal of Sustainable Development; Vol. 7, No. 1; 2014, ISSN 1913-9063 E-ISSN 1913-9071.

[20]. El-Sayed, M. A. H., 2005, "Solar supported steam production for power generation in Egypt," Energy Policy, 33(4), 1251-1259. http://dx.doi.org/10.1016/j.enpol.2003.11.021.

[21]. Khayet, M, 2013, "Solar desalination by membrane distillation: Dispersion in energy consumption analysis and water production costs (a review)," Desalination 308, pp. 89–101.

[22]. Nafey, A. S., Fath, H. E. S., and Mabrouk, A. A., 2006. "Thermoeconomic Analysis of Multi -Stage Flash-Thermal Vapor Compression (MSF-TVC) Desalination Process, "Tenth International Water Technology Conference, IWTC10 2006, Alexandria, Egypt.

[23]. Ziolkowska, J. R, 2015, "Is Desalination Affordable?— Regional Cost and Price Analysis," Water Resource Manage, Vol. 29, 1385-1897.